Slow Microtubule Binding Kinetics of Membrane-bound Kinesin Predicts High Motor Copy Numbers on Intracellular Cargo

Rui Jiang[1], Steven Vandal[2], SooHyun Park[3], Sheereen Majd[4], Erkan Tüzel[2], William O. Hancock[1,3]

[1]Intercollege Program in Integrative and Biomedical Physiology, Pennsylvania State University, University Park, PA 16802
[2]Department of Physics, Worcester Polytechnic Institute, Worcester, MA 01609
[3]Department of Biomedical Engineering, Pennsylvania State University, University Park, PA 16802
[4]Department of Biomedical Engineering, University of Houston, Houston, TX 77204

Classification: Biological sciences, Biophysics and Computational Biology

Corresponding Author:
William O. Hancock
420 CBEB
Pennsylvania State University
University Park, PA 16802
Email: woh1@psu.edu
Telephone: (814) 863-0492

Key Words: Kinesin-1 | lipid bilayers | kinetics | diffusion | long-range transport

Abstract
Bidirectional vesicle transport along microtubules is necessary for cell viability and function, particularly in neurons. When multiple motors are attached to a vesicle, the distance a vesicle travels before dissociating is determined by the race between detachment of the bound motors and attachment of the unbound motors. Motor detachment rates (k_{off}) can be measured via single-molecule experiments, but motor reattachment rates (k_{on}) are generally unknown, as they involve diffusion through the bilayer, geometrical considerations of the motor tether length, and the intrinsic microtubule binding rate of the motor. To understand motor attachment dynamics during vesicle transport, we quantified the microtubule accumulation rate of fluorescently-labeled kinesin-1 motors in a 2D system where motors were linked to a supported lipid bilayer. From the first-order accumulation rate at varying motor densities, we extrapolated a k_{off} that matched single-molecule measurements, and measured a two-dimensional k_{on}, which was considerably slower than expected based on the motor tether length. By incorporating cholesterol to reduce membrane diffusivity, we demonstrate that this slow k_{on} is not limited by the motor diffusion rate. Using a theoretical model to interpret our data and a computational model to simulate our experiments, we conclude that the slow k_{on} arises from the fact that motors bind to microtubules only from a small zone, measuring roughly the area of one tubulin dimer, close to the microtubule. The slow kinesin-1 on-rate predicts that long-range transport of membrane-bound vesicles *in vivo* requires tens to hundreds of motors per vesicle.

Significance Statement
Long-distance transport of membrane-coated vesicles involves coordination of multiple motors such that at least one motor is bound to the microtubule at all times. Microtubule attachment of a membrane-bound motor comprises two steps – diffusing through the lipid bilayer to a binding zone near the microtubule, followed by binding. Using a 2D supported lipid bilayer system, we show that membrane diffusion is not the limiting factor for motor attachment. Instead, motor attachment is intrinsically slow because motors must be very close to the microtubule to bind. This suggests that higher motor densities than previously anticipated are required for long-range vesicle transport, and that altering membrane composition to change motor diffusion is not an effective mechanism of bidirectional transport regulation.

Introduction
Survival and proper function of eukaryotic cells rely on the dynamics of numerous membranous organelles. Long-range transport of these cargos is carried out by the molecular motors kinesin and dynein, which walk towards the plus- (at cell periphery) and minus-ends (in perinuclear regions) of microtubules (MTs), respectively. Considerable work has been done to characterize the mechanochemical properties of kinesin and dynein by *in vitro* single-molecule studies (*1-3*). However, there is a significant knowledge gap between our understanding of *in vitro* motor biophysics and our understanding of *in vivo* vesicle transport. Generally, intracellular cargos have both kinesin and dynein simultaneously attached, and in a number of cases kinesins from multiple families are attached to the same cargo (*4-6*). Moreover, these motors are coupled through a lipid bilayer that surrounds the organelles, the effects of which have been studied only very recently (*5, 7-10*).

From a mechanical perspective, compared to attachment to a rigid surface, attachment to a lipid bilayer is expected to reduce motor performance because instead of moving the cargo along the microtubule, the motor can instead slip in the plane of the bilayer (*7*). On the other hand, being able to diffuse in the bilayer may enhance motor performance by allowing motors to diffuse to and accumulate on MTs.

Geometry may also play a role; in a study of *in vitro* vesicle transport driven by myosin Va motors, fluid-phase membranes led to faster transport velocities than gel-phase membranes, an effect attributed to optimal centering of the vesicles on remaining motors following detachment of the trailing motor (*8*). Cellular studies have also revealed a role for membrane composition in regulating motor function. For instance, the kinesin-3 family member KIF16B exists in a monomeric state, but binding to phosphatidylinositol-(3) monophosphate (PI(3)P) on membranous cargos through its Phox homology (PX) domain converts KIF16B into superprocessive dimers that drive cargo transport (*11*). As another example, early phagosomes move on MTs bidirectionally, but as they mature, cholesterol is increasingly incorporated into the membrane, which results in clustering of dyneins into microdomains. This clustering allows dyneins to work cooperatively to generate greater minus-end forces, resulting in increasingly minus-end directed movements of late phagosomes (*5*).

Despite growing appreciation of the role of lipid membranes in regulating cargo transport, the mechanisms by which long-range vesicle transport is achieved are not well understood. The average travel distance of a vesicle depends on the average number of engaged motors, which in turn is determined by a race between motor attachment and detachment rates (Fig. 1A). Motor detachment is described by the first-order off-rate k_{off}, which can be experimentally determined by dividing the single-molecule velocity by the run length (*12-14*). Measuring the motor attachment rate is more complicated because it involves two processes – diffusion of motors to a zone in which they are able to bind to the MT (described as a rate $k_{diffusion}$ into a binding zone with area A_{zone}), followed by MT binding, described by the first-order on-rate k_{attach}. Of these three parameters, k_{attach} for kinesin-1 has been measured in previous studies (*10, 12*), and bounds can be put on $k_{diffusion}$ based on the diffusion constant of motors in the bilayer. In contrast, the area of the zone in which motors can bind to the MT is less well constrained, though the motor's contour length provides an upper limit. How these parameters interact and whether cells modulate any or all of these parameters to regulate the speed and directionality of bidirectional transport are not understood. For instance, because different intracellular cargos have different lipid compositions (*15-17*), it is possible that the different diffusion constants alter motor binding kinetics and thus vesicle transport dynamics. This idea has not been experimentally tested, however.

To better understand the principles that govern cargo transport by vesicle-bound motors, we used a 2D lipid bilayer system to approximate the local membrane environment where motors attach to a MT (Fig. 1B). By measuring the rate of accumulation of membrane-bound kinesin-1 on MTs, we obtained a two-dimensional bi-molecular rate constant for motor attachment, k_{on_2D}, that was unexpectedly slow. By incorporating cholesterol to decrease the membrane diffusion constant, we revealed that this slow k_{on_2D} was not limited by membrane diffusion. Using both theoretical and computational approaches, we find that this surprisingly slow k_{on_2D} can be explained by a previously unanticipated small A_{zone} that was close to the surface area of one tubulin dimer. Based on these findings, we predicted that high motor densities are required for long-range vesicle transport.

Results and Discussion

Membrane-bound Kinesin-1 Motors Accumulate on Microtubules

To measure the interrelationship between membrane diffusional kinetics and motor binding kinetics, we visualized GFP-labeled motors diffusing in a supported lipid bilayer system by total internal reflection fluorescence (TIRF) microscopy (Fig. 1B). This 2D system closely resembles the interface between a MT and a large membranous cargo, where the local membrane curvature is negligible. A lipid bilayer composed of POPC with 0.1 – 0.6 mol% DSPE-PEG(2000)-Biotin was deposited on a cleaned glass

coverslip, and biotinylated GFP-labeled *Drosophila* kinesin-1 motors (K560GFP-AviC (*13*)) were linked to DSPE-PEG(2000)-Biotin through NeutrAvidin. Motor density was controlled by using saturating amounts of kinesin-1 pre-bound to Neutravidin, and varying the motor binding capacity of the bilayer by changing the percentage of DSPE-PEG(2000)-Biotin. MTs were introduced into the chamber and changes in kinesin-1 distribution upon MT landing were monitored by local increases in fluorescence from the GFP tag. The fluid lipid bilayer enabled motors to freely diffuse within the membrane, resulting in strong accumulation of kinesin-1 on MTs (Fig. 1C). In a control experiment using kinesin-1 immobilized on a glass surface, no co-localization between motors and MTs was seen.

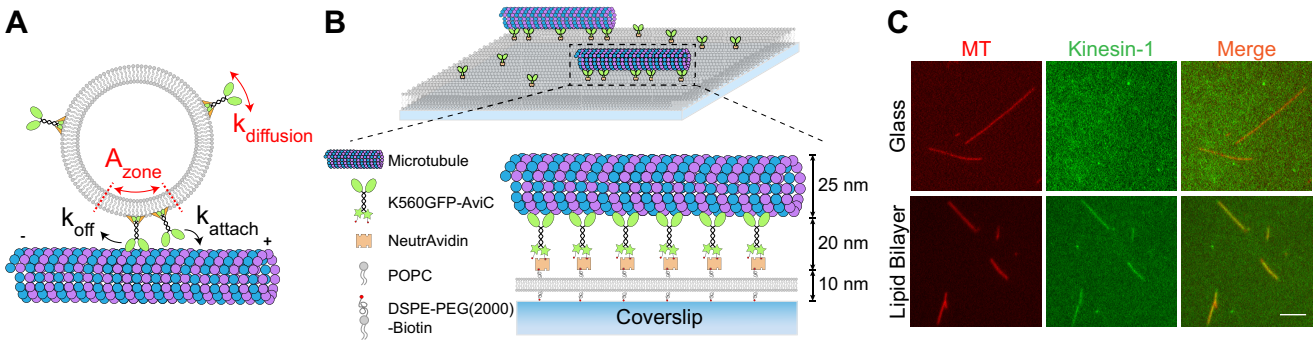

Fig. 1. Visualization of membrane-mediated motor re-organization in a 2D supported lipid bilayer system. (A) Key kinetic parameters that determine average vesicle travel distance include the motor diffusion rate to the MT ($k_{diffusion}$), the motor attachment rate (k_{attach}), and the motor off-rate (k_{off}). (B) Schematic illustrating linkage of biotinylated GFP-kinesin-1 (K560GFP-AviC) to DSPE-PEG(2000)-Biotin within a POPC lipid bilayer through NeutrAvidin. (C) Accumulation of membrane-bound kinesin-1 on MTs. Strong co-localization between kinesin-1 (green) and MTs (red) is seen only when kinesin-1 motors are bound to a lipid bilayer, not when motors are immobilized on a glass coverslip. Scale bar: 10 µm.

Determining Motor Binding Kinetics from the Accumulation Rate

To gain more insight into the kinetics of motor accumulation on the MT, we monitored the time course of motor fluorescence increase upon landing of a MT on the surface. Initially, motors were homogeneously distributed on the lipid bilayer, but upon MT landing, motors rapidly accumulated on MTs, reaching steady-state within seconds in the presence of 2 mM ATP (Movie S1, Fig. 2A). Consistent with a previous study (*7*), we observed MT gliding upon landing on the lawn of membrane-bound motors. To quantify motor accumulation, the integrated motor fluorescence in the region of the MT was fit to a single exponential function (Fig. 2C). We compared this motor accumulation rate constant, k_{acc}, across different motor densities, and found that k_{acc} scaled linearly with motor density on the membrane (Movie S1, Fig. 2A, Fig. 2C, blue and green curves, Fig. 2D, blue curve). k_{acc} varied from $0.86 \pm 0.05\ s^{-1}$ (mean ± SEM, N = 29) at low motor density (~700 motors/µm^2) up to $1.61 \pm 0.12\ s^{-1}$ (mean ± SEM, N = 35) at the highest motor density (~ 4400 motors/µm^2).

To understand k_{acc} in terms of motor binding and unbinding rates, we applied a simple kinetic model of membrane-bound kinesin motors (Kin) binding to the surface-bound MT, as follows:

$$Kin + MT \underset{k_{off}}{\overset{k_{on_2D}}{\rightleftharpoons}} Kin \cdot MT \qquad \textbf{[1]}$$

Here, k_{on_2D} is the two-dimensional bimolecular association rate constant and k_{off} is the first-order motor dissociation rate constant. This system is identical to a reversible bimolecular interaction in solution (*18*), with the difference that instead of units $M^{-1}s^{-1}$, k_{on_2D} has units (motors/µm^2)$^{-1}s^{-1}$. It can be shown (see Methods) that:

$$k_{acc} = k_{on_2D} \cdot [Kin]_{tot} + k_{off} \qquad \textbf{[2]}$$

Thus, for the curves in Fig. 2D, a linear regression of k_{acc} as a function of motor density yields a line with a slope equal to the bimolecular on-rate, k_{on_2D}, and a y-intercept equal to the first-order motor off-rate, k_{off}. The fitted k_{off} of $0.8 \pm 0.6\ s^{-1}$ (mean ± 95% confidence bound of fit) was in good agreement with previous single-molecule measurements for these motors in saturating ATP, where k_{off} = velocity/run length (*14, 19*). From the linear fit, k_{on_2D} in saturating ATP was $1.8 \pm 2.4 \times 10^{-4}$ $(motor/\mu m^2)^{-1}s^{-1}$ (mean ± 95% confidence bound of fit).

One prediction of this model is that if we change the k_{off} without changing the k_{on_2D}, then the slope should be unaffected, and only the y-intercept should change. To test this prediction, we measured k_{acc} in the presence of 2 mM AMPPNP (Movie S1, Fig. 2B, Fig. 2C, red and magenta curves), instead of ATP. This non-hydrolyzable ATP analog prevents kinesin-1 dissociation from MT, thus reducing k_{off} to $0\ s^{-1}$. Because ADP release is rate-limiting for kinesin in solution, the bimolecular interaction determining the k_{on_2D} should be identical for the two nucleotides. As shown in the red curve in Fig. 2D, k_{acc} scaled linearly with motor density in AMPPNP, k_{off} was $0.0 \pm 0.4\ s^{-1}$ as expected, and the k_{on_2D} of $2.8 \pm 2.0 \times 10^{-4}$ $(motor/\mu m^2)^{-1}s^{-1}$ was similar to that in ATP. Thus, we have directly measured for the first time to our knowledge, the bimolecular on-rate for membrane-bound motors binding to MTs. As shown below, this parameter allows one to predict the travel distance of a vesicle with known size, motor number (from which motor density can be calculated), and motor k_{off}.

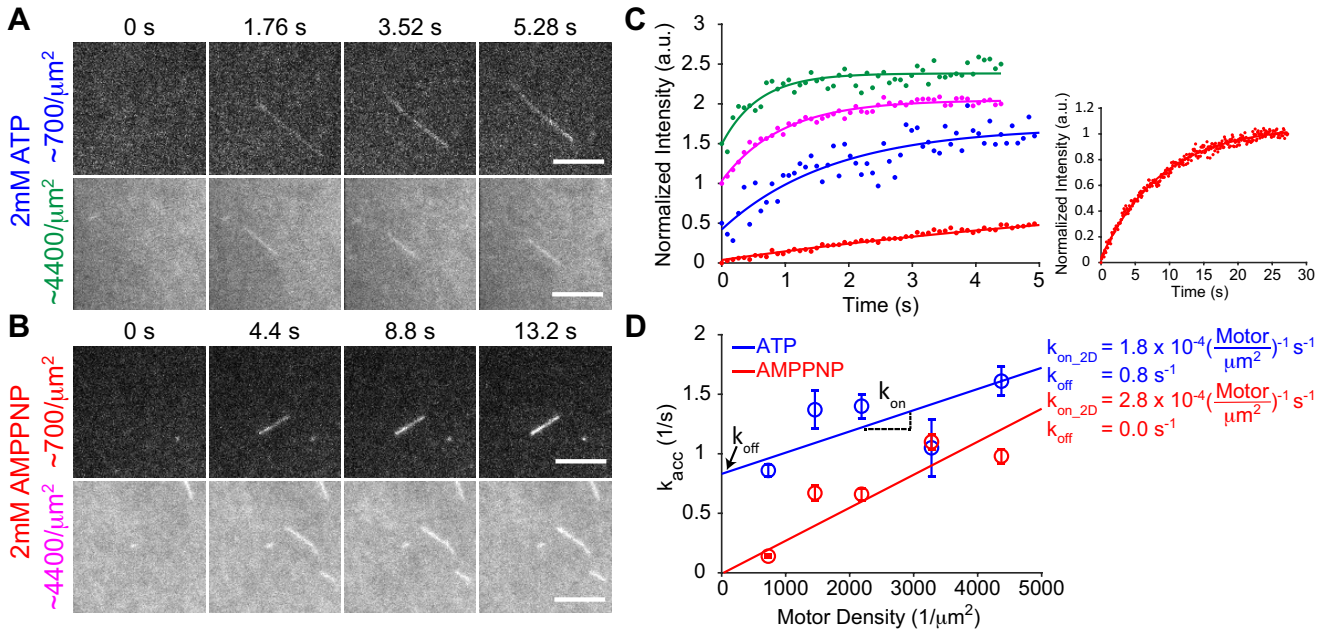

Fig. 2. Quantification of k_{on_2D} from the accumulation process. (A,B) Time-lapse snapshots of motor accumulation in 2 mM ATP (A) or 2 mM AMPPNP (B) at low (~700 motors/μm^2) or high (~4400 motors/μm^2) motor densities. Upon MT landing at 0 s, the initially homogeneously distributed motors accumulate on the MT. Scale bar: 5 μm. (C) Time courses of integrated GFP intensity on MTs, with single exponential fit, color-coded for examples shown in (A,B). Inset: The entire curve (30 s) for the example in 2 mM AMPPNP at ~700 motors/μm^2. Raw intensity is normalized and offset by 0.5 for visualization. (D) Accumulation rate (k_{acc}, from exponential fits in C) versus kinesin-1 density in 2 mM ATP (blue) or 2 mM AMPPNP (red). Each data point represents mean of 6-38 measurements. Error bars indicate SEM.

Motor Attachment is Not Limited by Membrane Diffusion

The accumulation of membrane-bound motors on the microtubule can be considered as two sequential steps – motor diffusion ($k_{diffusion}$) into a binding zone near the MT (A_{zone}), followed by motor attachment to MT (k_{attach}) from this binding zone (Fig. 1A). Depending on the diffusion constant and distance

covered, k_{on_2D} could in principle be determined by either the motor diffusion rate or the motor on-rate when near the MT. Because different vesicle populations are known to have different lipid compositions (*16, 17, 20*), motor diffusivity could be a potential regulator of motor activity in cells. To investigate whether diffusion or binding is rate-limiting for motor accumulation, we decreased the motor diffusion constant by incorporating 30 mol% cholesterol into the POPC lipid bilayer. Fluorescence recovery after photobleaching (FRAP) measurements indicated that cholesterol incorporation resulted in a 3.8-fold decrease in the lipid diffusion coefficient (0.25 ± 0.03 $\mu m^2/s$ versus 0.95 ± 0.14 $\mu m^2/s$ for control; mean ± SD, N = 6 bilayers for each; Fig. 3A, Movie S2). We next quantified motor accumulation rate as a function of motor density in 2 mM ATP or AMPPNP on lipid bilayers containing 30% cholesterol (Fig. 3B, C). Addition of cholesterol into the membrane did not alter the motor attachment rate (k_{on_2D} = 2.9 ± 4.1 × 10^{-4} $(motors/\mu m^2)^{-1}s^{-1}$ in ATP, and 2.7 ± 1.5 × 10^{-4} $(motors/\mu m^2)^{-1}s^{-1}$ in AMPPNP). This result seems surprising, but on closer inspection makes sense, as follows. If we assume that the zone from which motors can bind to the MT extends 50 nm on either side of the MT (roughly the kinesin tether length (*21-23*)), then from the 1D diffusion equation $x^2 = 2Dt$, it should take motors an average of 1.3 ms (control) or 5.0 ms (plus cholesterol) to diffuse into and out of the zone. These times convert to rate constants orders of magnitude faster than 0.8 s^{-1} kinesin-1 off-rate, meaning that following detachment (or equivalently following attachment), motor populations inside and outside the binding zone will rapidly equilibrate. We therefore conclude that under our conditions, motor attachment to the MT is not limited by membrane diffusion. This suggests that kinesin-1 MT binding kinetics remain the same, regardless of membrane fluidity/composition of cargos, unless they are organized into higher-order structures.

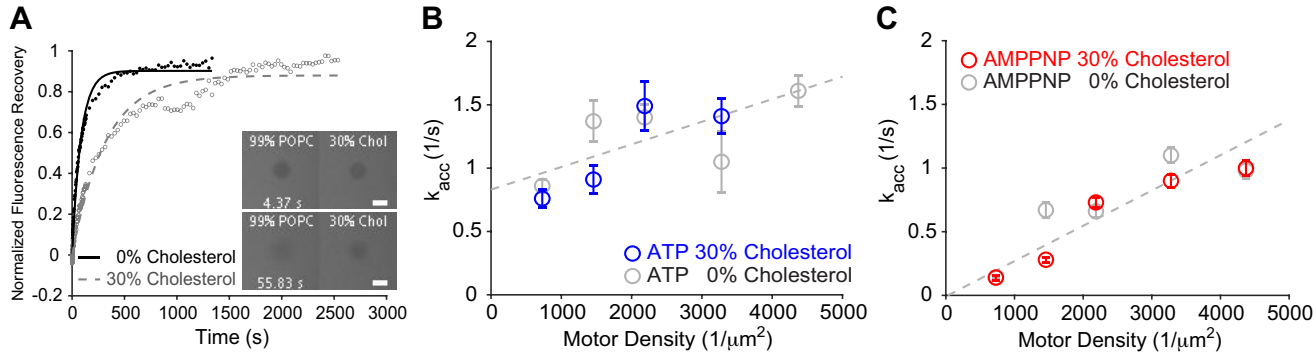

Fig. 3. k_{on_2D} of membrane-bound motors is not determined by membrane diffusion. (A) Example traces of fluorescence recovery after photobleaching (FRAP) measurement of lipid bilayers without (black) or with 30% cholesterol (gray). Diffusion coefficients were calculated as 0.96 $\mu m^2/s$ and 0.25 $\mu m^2/s$, respectively, from single exponential fitting. Scale bar: 30 μm. (B,C) Motor accumulation rate versus kinesin-1 density in 2 mM ATP (B) or 2 mM AMPPNP (C) in the presence or absence of cholesterol in the membrane. Each data point with cholesterol represents mean of 12-73 measurements; control data in gray taken from Fig. 2C. Error bars indicate SEM.

Measured On-rate Predicts a Small Binding Zone

To better understand our observed motor accumulation kinetics and to relate them to the physiological case of spherical vesicles of varying diameters, we developed an analytical model of the motor accumulation process. Because the motor diffusion rate within the membrane is considerably faster than motor binding kinetics, we made the assumption that the pool of motors within the binding zone is in rapid equilibrium with the pool of motors outside the binding zone. From our measured parameters k_{on_2D} and σ, the 2D bimolecular on-rate and the motor surface density, respectively, the flux of motors binding to the MT (in motors/s) is equal to $k_{on_2D} \cdot \sigma$ (equivalent to $k_{on} \cdot$[motor] in solution). If we consider only those motors within the binding zone of a given tubulin subunit, then we can calculate an equivalent motor flux onto the MT as the number of motors in the zone, N, multiplied by a first-order

motor attachment rate, k_{attach}. In this case, the number of motors in the zone, N, is equal to $\sigma \cdot A_{zone}$, where σ is the motor density and A_{zone} is the area. Uniting these two representations of the motor flux onto the MT,

$$k_{on_2D} \cdot \sigma = k_{attach} \cdot \sigma \cdot A_{zone} \quad \textbf{[3]}$$

Thus,

$$k_{on_2D} = k_{attach} \cdot A_{zone} \quad \textbf{[4]}$$

Our experimentally determined k_{on_2D} was 2.3×10^{-4} (motor/μm^2)$^{-1}$s^{-1} (mean of measurements in ATP and AMPPNP). The first-order kinesin attachment rate, k_{attach} has been previously calculated from a lipid vesicle system to be 4.7 s^{-1} (*10*) and from a DNA scaffold system to be 4.6 s^{-1} (*12*). Although the 2D lipid bilayer system is a third geometry, we make the tentative assumption that the first-order on-rate also applies here. Thus, we can calculate an estimate for the area around a given tubulin subunit from which motors can bind as A_{zone} = 50 nm^2. This value is considerably smaller than the ~8000 nm^2 area predicted by a model in which all of the motors within a 50 nm motor contour length can bind to a given tubulin, an approach that was taken by others (*5, 24*). Interestingly, this 50 nm^2 is not far from the (8 nm × 4 nm = 32 nm^2) projected surface area of a tubulin dimer (Fig. 5A).

Simulations Verify Small Binding Zone and Independence of Accumulation Rate on Membrane Diffusion

To verify our analytical result, we carried out simulations that incorporated motor diffusion within the membrane, motor on/off binding kinetics, and mechanical interactions between motors bound to the same MT (*25*). The simulation initiated upon landing of a MT on a lawn of kinesin-1 motors of varying densities diffusing on a lipid bilayer with D = 1 μm^2/s. Motor binding was described with first-order attachment rate, k_{attach} of 5 s^{-1}, when there were available binding sites within its reach distance, d_{bind} (Fig. 4A). The simulated accumulation rate matched well with experimental measurements using a reach distance of 3.1 nm (Fig. 4B), which corresponded to an A_{zone} of 50 nm^2 (A_{zone} = 8 nm × d_{bind} × 2, Fig. 4A). In contrast, when using d_{bind} of 17 nm or 80 nm, corresponding to the distance kinesin-1 holds its cargo above the surface (*21*) and kinesin-1's contour length (*22, 23*), respectively, the motor accumulation rate was significantly overestimated. Therefore, our simulations support our analytical result that kinesin-1 only binds to the nearest tubulin dimer (Fig. 5A). It follows that assuming kinesin-1 can access all of the tubulin binding sites within the contour length of its coiled-coil (or anything greater than the dimensions of tubulin) leads to an overestimate of motor flux onto the MT, and thus an underestimate of the number of motors needed to carry a cargo long distances.

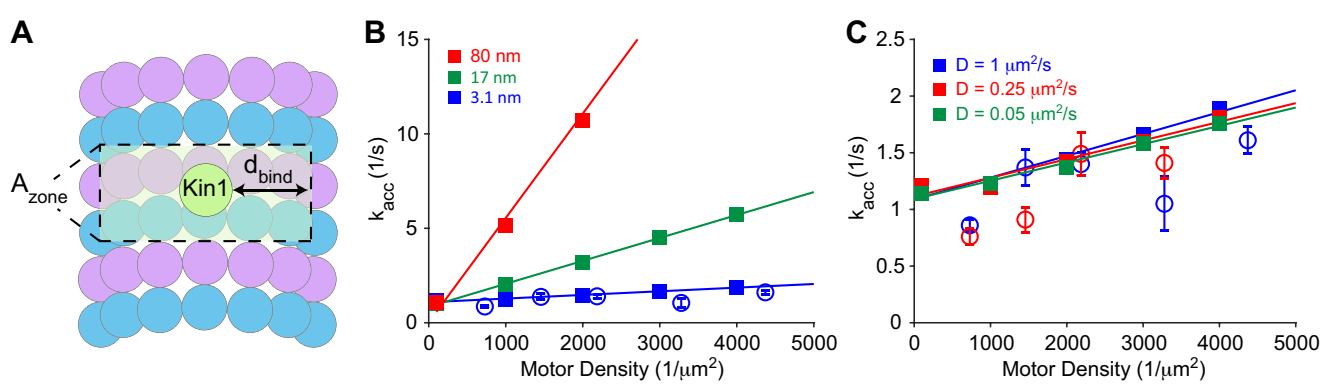

Fig. 4. Simulation of motor accumulation. (A) Diagram illustrating conversion between A_{zone} and d_{bind}. (B) Accumulation rate with different motor reach distances; experimental data shown in blue open circles. (C) Accumulation rate at varying membrane diffusivities, using 3.1 nm reach distance; experimental data shown in blue (no cholesterol) and red (30% cholesterol) open circles.

After constraining the motor binding distance, d_{bind}, we simulated motor accumulation behavior at reduced membrane fluidities. Consistent with experimental data, the motor accumulation rate was not altered when membrane diffusion was reduced by 4-fold (Fig. 4C). Moreover, the accumulation rate remained unchanged when membrane diffusion was reduced by 20-fold, further supporting that the rate of MT binding is limited by the interaction between the motor head with the MT, rather than motor diffusion in the membrane.

Slow Attachment Predicts High Motor Densities for Long-range Vesicle Transport

Achieving run lengths greater than the single-motor distance requires multiple motors on a cargo simultaneously binding to the MT such that when one motor dissociates, others are there to continue transport. Using the kinetic parameters measured here, we carried out simulations to predict the number of kinesin-1 motors required to achieve long-range transport of vesicles of varying diameters. The vesicle motor density, σ, was defined as the number of motors on the vesicle divided by the membrane surface area of the vesicle. The flux of vesicle-bound motors binding to the MT was defined as $k_{on_2D} \cdot \sigma$, and the flux of motors detaching from the MT was determined by k_{off} times the number of MT-bound motors. A naïve prediction of this system is that for vesicles smaller than the motor contour length, every motor can access any MT, so having multiple motors on a vesicle leads to longer run lengths. However, analogous to the slow accumulation in the supported lipid bilayer system, we found that high motor densities on the vesicle are necessary for there to be a substantial probability that when a motor dissociates from the MT, a second attached motor is there to maintain transport. For instance, a 30 nm vesicle needed 14 motors to travel 10 µm (Fig. 5B). Larger vesicles require even more motors to achieve these long transport distances – 70 nm and 100 nm require 57 and 108 motors, respectively, to travel the same distance.

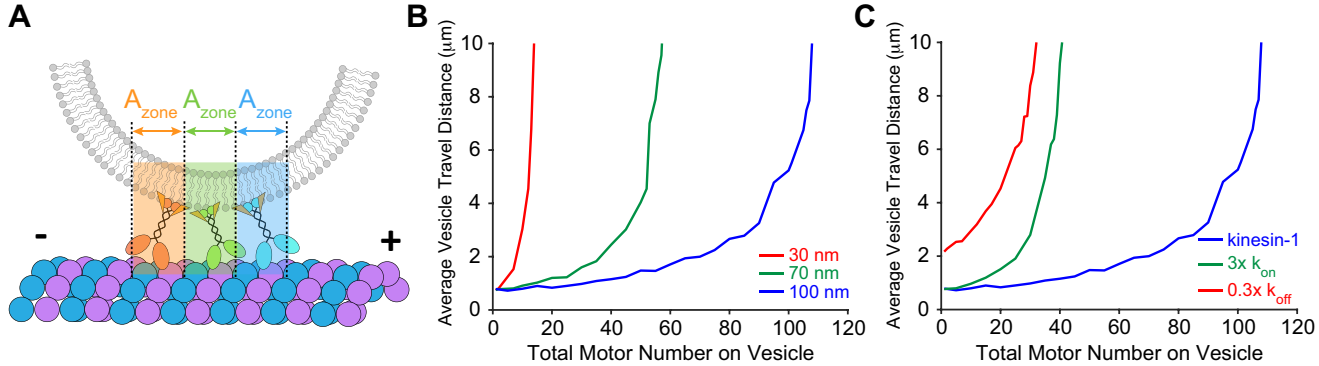

Fig. 5. Slow motor attachment rate predicts high motor density for long-range vesicle transport. (A) Slow motor attachment can be explained by a model in which kinesin-1 only binds to the nearest tubulin dimer (A_{zone} matches area of tubulin dimer). (B) Simulation of vesicle travel distance versus motor number per vesicle for vesicles of varying diameters. (C) Simulation of travel distance versus motor number for a 100 nm vesicle, using a different first-order motor binding rate when in the binding zone or a different off-rate.

Although this requirement for high motor numbers per vesicle seems surprising, it is in fact consistent with a number of published optical trap experiments, where single-molecule activity is routinely achieved by incubating beads with a thousand-fold excess of motors (*26, 27*). For vesicles larger than the motor contour length, motor-MT interactions are naturally geometrically constrained; for instance it has been calculated that for a 760 nm diameter vesicle, only 4% of dynein randomly distributed on the surface can reach the MT, assuming a dynein contour length of 70 nm (*5*). Our conclusion that the binding zone for a motor is much less than its contour length shifts this percentage down considerably and provides a kinetic description of the process.

The high motor copy number per vesicle that we predict contrasts with previous measurements of neuronal vesicles that found on average three dynein, one kinesin-1, and two kinesin-2 motors attached to a 90 nm vesicle (*6*). Notably, vesicles in this and related studies generally display pauses and diffusive episodes that are consistent with tethering events when no motors are functionally attached to the microtubule. To account for these low motor numbers, we hypothesize that teamwork between motors from different families that have varying binding kinetics and the ability to tether through electrostatic interactions could improve transport efficiency and reduce the number of motors required for long-range transport. For instance, kinesin-2 has been shown to have a 4-fold faster k_{on} compared to kinesin-1, suggesting it may play a tethering role to maximize attachment of a vesicle to the MT (*12*). Also, activated mammalian dynein has an off-rate on the order of 0.04 s^{-1} (*28*), meaning that slowly detaching dyneins can hold a vesicle near the MT, enabling kinesins that detach to rapidly rebind and continue bidirectional transport. To test this hypothesis, we ran the simulations where we varied k_{on} or k_{off} and found that transport efficiency increased drastically with either a 3-fold faster k_{on} or 3-fold slower k_{off} (Fig. 5C). Finally, dynein has been shown to cluster into microdomains in late phagosomes (*5*), which is expected to increase its k_{on} dramatically because motors no longer diffuse in the membrane and their clustering significantly increases the local motor concentration.

Conclusions

Organelles and other membranous cargos need to travel tens of μm or longer to reach their destinations, which is achieved by the teamwork in a group of motors that only travel several μm individually. The distance that a cargo can travel is ultimately determined by the race between attachment of the free motors and detachment of the bound motors. In this study, we dissected four key parameters in this kinetic process. From the motor accumulation on a lipid bilayer, we measured k_{off}, which matches with previous single-molecule studies, and the two-dimensional bimolecular on-rate, k_{on_2D}, which is related to: i) the membrane diffusion rate $k_{diffusion}$, ii) the binding zone A_{zone} within which motors can access the MT, and iii) k_{attach}, the first-order attachment rate when motors are within the binding zone. k_{on_2D} remained unchanged when membrane diffusivity was reduced by cholesterol, indicating that motor attachment is not limited by membrane diffusion and suggesting that changes in membrane fluidity are not a mechanism by which cells can regulate transport properties of different vesicle cargos. Using the reported value of k_{attach}, both our theoretical and computational work suggest an A_{zone} much smaller than that predicted by the motor contour length, and one that is close to the area of a tubulin dimer. This small zone of interaction explains the intrinsically slow binding of kinesin-1 to the MT and the prediction that high motor densities is required for long-range vesicle transport. This work leaves open the possibility some vesicles achieve long-distance transport by clustering motors in membrane microdomains or through scaffold proteins. As suggested from recent work on dynein (*5*), this clustering may be a mechanism to regulate motor directionality during bidirectional transport in cells.

Materials and Methods

Protein Constructs and Purification

The K560GFP-AviC construct was made by inserting the biotin ligase consensus sequence (AviTag) (*13*) between the eGFP tag and the 6x His tag in a previously described K560GFP construct (*12*). Insertions were carried out using Q5 site-directed mutagenesis (New England Biosciences). Motors were expressed polycistronically with BirA biotin ligase, in BL21 (DE3) bacteria (New England Biosciences) and purified by affinity chromatography, as previously described (*12, 13, 29*). Motor concentration was quantified by GFP absorbance or fluorescence at 488 nm.

Formation of Supported Lipid Bilayers (SLBs)
1-palmitoyl-2-oleoyl-glycero-3-phosphocholine (POPC), 1,2-disteroyl-*sn*-glycero-3-phosphoethanolamine-N-[biotinyl(polyethylene glycol)-2000] (DSPE-PEG(2000)-Biotin) and cholesterol were purchased from Avanti. Lipids were dissolved in chloroform and mixed in desired molar ratio. 1,2-dioleoyl-*sn*-glycero-3-phosphoethanolamine labeled with Atto 647N (Atto 647N DOPE) (Sigma) was incorporated into all lipid bilayers for visualization. Lipid composition without cholesterol was POPC:DSPE-PEG(2000) Biotin:Atto 647N DOPE at 99:0.1-1:0.05, and the composition with cholesterol was POPC:cholesterol:DSPE-PEG(2000) Biotin:Atto 647N DOPE at 69:30:0.1-1:0.05. The bulk of chloroform in the lipid mixture was evaporated in a rotary evaporator for 1.5 h. Lipids were left under vacuum for another 3 h to remove any trace chloroform. The dry lipid film was rehydrated in BRB80 (80 mM Pipes, 1 mM EGTA, 1 mM $MgCl_2$; pH 6.9) to a final lipid concentration of 0.5 mg/ml, and the lipid suspension was subjected to 10 freeze-thaw cycles in liquid nitrogen and warm water bath. Small unilamellar vesicles (SUVs) were formed by passing the lipid solution 11 times through a 100 nm polycarbonate membrane, followed by 21 times through a 30 nm membrane, using a mini-extruder (Avanti).

Glass coverslips (#1.5, 24×30 mm, Corning) were cleaned as previously described (*30*). Coverslips were boiled in 7x detergent (MP Biomedicals) diluted 1:7 with 18.2 MΩ water for 2 h. Coverslips were then rinsed thoroughly with 18.2 MΩ water, blown dry with nitrogen, and annealed at 550 ℃ for 6 h. Coverslips were cleaned by a plasma cleaner (Harrick Plasma) immediately before formation of SLBs. Polydimethylsiloxane (PDMS) spacers were made using Sylgard 184 silicone elastomer kit (Dow Corning). Cured PDMS was cut by a biopsy punch (Acuderm) to make spacers 6 mm inner diameter and ~2 mm thick that were adhered to clean coverslips. 50 µl SUVs was added to the well and incubated for 10 min, followed by thorough wash in BRB80 to remove excess SUVs.

Accumulation Assay
Taxol-stabilized microtubules (MTs) were polymerized from bovine brain tubulin, as described previously (*12-14, 29*). Rhodamine-labeled MTs (rhodamine:unlabeled = 1:3) were used in experiments in Fig. 1C, unlabeled MTs were used otherwise. MTs were sheared by passing twice through a 30g needle. Motor-functionalized bilayers were formed by binding pre-formed kinesin-NeutrAvidin complexes to biotinylated lipid bilayers, as follows. 200 nM kinesin was incubated with 2 µM NeutrAvidin (Thermo Scientific) in BRB80 containing 100 µM AMPPNP, 10 µM taxol, and 1 mM DTT for 10 min at room temperature (RT). Excess of NeutrAvidin ensured that all biotinylated motors were occupied, without cross-linking of motors. To remove excess NeutrAvidin, the solution was incubated 10 min with 1 µM MT, centrifuged for 10 min in an Airfuge (Beckman-Coulter), inactive motors and excess NeutrAvidin in the supernatant were discarded. The pellet containing MTs with bound kinesin-NeutrAvidin (K-NA) was resuspended in motor buffer (1 µM taxol, 2 mM ATP, 20 mM D-glucose, 1 mM DTT in BRB80), incubated for 10 min at RT to release active motors, followed by an Airfuge spin to remove MTs with irreversibly bound motors.

SLBs were equilibrated with motor buffer, 50 µl of K-NA solution was then introduced, followed by a 10 min incubation to allow motors to bind to the SLB. Excess motors were removed by a wash of motility buffer (1 µM taxol, 2 mM ATP or AMPPNP, 1 mM DTT, 40 mM D-glucose, 0.02 mg/ml glucose oxidase, 0.008 mg/ml catalase in BRB80). 16-32 nM MTs in motility buffer were introduced immediately before imaging, and accumulation of GFP-labeled motors was imaged using a Nikon

TE2000 TIRF microscope (except for Fig. 1C, which was captured using an epifluorescence microscope), as described previously (*14*).

Control and Calculation of Surface Motor Density

To ensure full motor occupancy of DSPE-PEG(2000)-Biotin, SLBs containing 1% DSPE-PEG(2000)-Biotin were always included in the experiments but discarded in data analysis. GFP intensity from motors on SLBs with 1% DSPE-PEG(2000)-Biotin was always stronger than that on SLBs with less DSPE-PEG(2000)-Biotin, indicating the amount of K-NA saturated all the binding sites on SLBs with 0.1-0.6% DSPE-PEG(2000)-Biotin. Surface motor density was calculated by multiplying the density of biotin binding sites on the SLB and motor activity. Surface lipid density was calculated using a surface area of lipid head group of 0.7 nm^2. Biotin densities on the SLBs were then calculated based on the molar ratio of DSPE-PEG(2000)-Biotin. 0.1% and 0.6% DSPE-PEG(2000) Biotin thus corresponded to surface biotin density of 1429 and 8571 biotin/μm^2, respectively. Motor activity within the K-NA complexes were quantified by comparing the ATPase activity of the complex to that of kinesin-1 without NeutrAvidin by ATPase assay, as described previously (*29, 31*). Kinesin-1 activity within the K-NA complexes were measured to be 51 ± 13 % (mean ± SD), therefore, 0.1% and 0.6% DSPE-PEG(2000) Biotin corresponded to active surface motor density of 729 and 4371 motors/μm^2, respectively.

Analytical model for motor accumulation rate

The motor accumulation rate in Fig. 2 was analyzed as follows. The rate of production of Kin·MT complex can be expressed as:

$$\frac{d[Kin \cdot MT]}{dt} = k_{on_2D} \cdot [Kin] \cdot [MT] - k_{off} \cdot [Kin \cdot MT] \quad \textbf{[5]}$$

If the assumption is made that the fraction of MT-bound kinesin-1 is negligible compared to the total pool of membrane-bound motors (i.e. $[Kin]_{tot}$ » [Kin·MT]), Eq. **5** can be re-written to:

$$\int_0^{[Kin \cdot MT]} \frac{d[Kin \cdot MT]}{[MT]_{tot}/(1+k_{off}/(k_{on_2D} \cdot [Kin]_{tot}))} = \int_0^t (k_{on_2D} \cdot [Kin]_{tot} + k_{off}) \cdot dt \quad \textbf{[6]}$$

where $[MT]_{tot}$ is the total concentration of motor binding sites on the MT. Eq. **6** can be solved for the timecourse of motor on the MT:

$$[Kin \cdot MT] = \frac{[MT]_{tot}}{1+k_{off}/(k_{on_2D} \cdot [Kin]_{tot})} (1 - e^{-(k_{on_2D} \cdot [Kin]_{tot} + k_{off}) \cdot t}) \quad \textbf{[7]}$$

thus,

$$k_{acc} = k_{on_2D} \cdot [Kin]_{tot} + k_{off}$$

Fluorescence Recovery After Photobleaching (FRAP)

To obtain sufficient signal-to-noise ratio for FRAP measurement, 0.5 mol% Atto 647N DOPE was incorporated into SLB samples. Images were captured using a Nikon Eclipse Ti microscope equipped with a Plan Apo 10x DIC N1 objective and an attached digital complementary metal-oxide semiconductor (CMOS) camera (ORCA-Flash 4.0 V2, Hamamatsu) in conjunction with NIS-Elements (Nikon) software. SLBs were excited with a 640 nm light source (Aura II, Lumencor). A 15 mW 561 nm laser (LU-N3 Laser Unit, Nikon) equipped with a Bruker Miniscanner was used to bleach Atto 647N DOPE at 50-80% output power for 3 s. The laser beam had an effectively cylindrical profile with a

diameter of 30 μm. To minimize photobleaching during recovery, images were captured immediately after bleaching every 40-60 ms for 2 s, then every 500 ms for 10 s, followed by every 3 s for 2 min, and finally switched to every 30 s. Data analysis was carried out as previously described (*30*), using a correction factor of 1.

Data Analysis

Accumulation image sequences were analyzed in Fiji (*32*). The trace that a newly landing MT glided along was tracked manually and the GFP intensity profile along the trace was plotted over time. The frame that the MT landed was defined by the slope maximum on a plot of average GFP intensity along the trace versus time. After background correction, the trace was fitted by a single exponential function from which k_{acc} was obtained. A weighted (by inverse of SEM) linear regression between k_{acc} and surface active motor density by linear least square fitting was carried out in MATLAB (The MathWorks).

Coarse-grained Simulation of Motor Accumulation

Our simulation of motors accumulating on MTs gliding over a lipid bilayer is a two-dimensional coarse-grained model with discrete time steps. The simulation consists of a patch of lipid bilayer with periodic boundary conditions, on which kinesin-1 motors diffuse. The motors are initially randomly distributed at a specified surface density, and act as point particles subject to Brownian forces from the lipid; in the *x*- and *y*-directions the Brownian force is normally distributed with a mean of zero and a standard deviation of $\sqrt{2k_BT\xi_{kin}/\Delta t}$, where k_BT is the thermal energy, ξ_{kin} is the friction coefficient of the motor, and Δt is the time step of the simulation. The MT diffuses two-dimensionally in solution, subjected to Brownian forces and torques about its center of mass.

For each time step of the simulation, the position of the motors and MT are updated based on the forces to which they are subjected following a discretized Langevin equation, $\Delta x_i = F_i \Delta t/\xi_i$, where Δx_i is the change in position in the x_i direction, F_i is the net force in that direction, and ξ_i is the drag coefficient of the motor or MT under question in that direction. If a motor is within its specified binding distance d_{bind} of a protofilament, it has a chance of binding to the closest binding site on that protofilament, determined by the first-order on-rate k_{attach}.

Once bound to the MT, the motor feels a force that depends on the distance between its head and its distal attachment point, which for a cable-like spring is given by $F_{kin} = \kappa(\ell - \ell_0)\Theta(\ell - \ell_0)$ where κ is the spring constant of the motor, ℓ is the motor's current length, ℓ_0 is the motor's contour length, and Θ is a Heavyside step function. The motor steps to the next binding site of the protofilament with a velocity determined by the component of this force parallel to the MT $F_{\parallel}$; if the motor is under an assisting force the motor walks with its unloaded stepping velocity v_u, and if the motor is under a hindering force it steps with a probability determined by the velocity $v = v_u\left(1 - \frac{F_{\parallel}}{F_s}\right)$ where F_s is the stall force of the motor. Additionally, the motor may unbind from the protofilament with a force-dependent off rate. The force exerted by the motor is applied to the MT as well as to the motor's diffusing lipid-bound tail; this force enters the discretized Langevin equation when calculating the motor's and MT's updated positions. The simulation calculates the new state of the simulation for each consecutive time step until a specified stopping time.

Simulation of Vesicle Transport.

Vesicle transport was simulated by modifying a MATLAB code that was previously used to simulate single-molecule runs (*29*). Each state was defined by the number of engaged motors instead of a step within one hydrolysis cycle. Average vesicle transport distance was calculated by multiplying the simulated dwell time and kinesin-1 velocity of 600 nm/s (*13*).

Acknowledgements
We are grateful to David Arginteanu for his help with protein preparation, Paul Cremer and Simou Sun for advice on supported lipid bilayers, Codey Henderson for assistance on FRAP experiments, and members from Hancock laboratory and Cremer laboratory for helpful discussions.
This work was funded by National Institutes of Health (NIH) grant R01 GM121679 to W.O.H. and E.T. R.J. was supported by NIH T32 GM108563.

Author Contributions
R.J., W.O.H. designed research; R.J., S.V., S.P. performed research; R.J., S.V., E.T. and W.O.H. analyzed data; and R.J. and W.O.H. wrote the paper.

References
1. W. O. Hancock, The Kinesin-1 Chemomechanical Cycle: Stepping Toward a Consensus. *Biophys J* **110**, 1216-1225 (2016).
2. D. A. Grotjahn *et al.*, Cryo-electron tomography reveals that dynactin recruits a team of dyneins for processive motility. *Nat Struct Mol Biol* **25**, 203-207 (2018).
3. L. Urnavicius *et al.*, Cryo-EM shows how dynactin recruits two dyneins for faster movement. *Nature* **554**, 202-206 (2018).
4. G. T. Shubeita *et al.*, Consequences of motor copy number on the intracellular transport of kinesin-1-driven lipid droplets. *Cell* **135**, 1098-1107 (2008).
5. A. Rai *et al.*, Dynein Clusters into Lipid Microdomains on Phagosomes to Drive Rapid Transport toward Lysosomes. *Cell* **164**, 722-734 (2016).
6. A. G. Hendricks *et al.*, Motor coordination via a tug-of-war mechanism drives bidirectional vesicle transport. *Curr Biol* **20**, 697-702 (2010).
7. R. Grover *et al.*, Transport efficiency of membrane-anchored kinesin-1 motors depends on motor density and diffusivity. *Proc Natl Acad Sci U S A*, (2016).
8. S. R. Nelson, K. M. Trybus, D. M. Warshaw, Motor coupling through lipid membranes enhances transport velocities for ensembles of myosin Va. *Proc Natl Acad Sci U S A* **111**, E3986-3995 (2014).
9. D. R. Klopfenstein, M. Tomishige, N. Stuurman, R. D. Vale, Role of phosphatidylinositol(4,5)bisphosphate organization in membrane transport by the Unc104 kinesin motor. *Cell* **109**, 347-358 (2002).
10. C. Leduc *et al.*, Cooperative extraction of membrane nanotubes by molecular motors. *Proc Natl Acad Sci U S A* **101**, 17096-17101 (2004).
11. V. Soppina *et al.*, Dimerization of mammalian kinesin-3 motors results in superprocessive motion. *Proc Natl Acad Sci U S A* **111**, 5562-5567 (2014).
12. Q. Feng, K. J. Mickolajczyk, G. Y. Chen, W. O. Hancock, Motor Reattachment Kinetics Play a Dominant Role in Multimotor-Driven Cargo Transport. *Biophys J* **114**, 400-409 (2018).
13. K. J. Mickolajczyk *et al.*, Kinetics of nucleotide-dependent structural transitions in the kinesin-1 hydrolysis cycle. *Proc Natl Acad Sci U S A* **112**, E7186-7193 (2015).

14. S. Shastry, W. O. Hancock, Neck linker length determines the degree of processivity in kinesin-1 and kinesin-2 motors. *Curr Biol* **20**, 939-943 (2010).
15. P. Sanghavi *et al.*, Coin Tossing Explains the Activity of Opposing Microtubule Motors on Phagosomes. *Curr Biol*, (2018).
16. N. Rocha *et al.*, Cholesterol sensor ORP1L contacts the ER protein VAP to control Rab7-RILP-p150 Glued and late endosome positioning. *J Cell Biol* **185**, 1209-1225 (2009).
17. G. van Meer, D. R. Voelker, G. W. Feigenson, Membrane lipids: where they are and how they behave. *Nat Rev Mol Cell Biol* **9**, 112-124 (2008).
18. T. D. Pollard, E. M. De La Cruz, Take advantage of time in your experiments: a guide to simple, informative kinetics assays. *Mol Biol Cell* **24**, 1103-1110 (2013).
19. K. J. Mickolajczyk, W. O. Hancock, Kinesin Processivity Is Determined by a Kinetic Race from a Vulnerable One-Head-Bound State. *Biophys J* **112**, 2615-2623 (2017).
20. D. Pathak, R. Mallik, Lipid - Motor Interactions: Soap Opera or Symphony? *Curr Opin Cell Biol*, (2016).
21. J. Kerssemakers, J. Howard, H. Hess, S. Diez, The distance that kinesin-1 holds its cargo from the microtubule surface measured by fluorescence interference contrast microscopy. *Proc Natl Acad Sci U S A* **103**, 15812-15817 (2006).
22. J. M. Scholey, J. Heuser, J. T. Yang, L. S. Goldstein, Identification of globular mechanochemical heads of kinesin. *Nature* **338**, 355-357 (1989).
23. N. Hirokawa *et al.*, Submolecular domains of bovine brain kinesin identified by electron microscopy and monoclonal antibody decoration. *Cell* **56**, 867-878 (1989).
24. R. P. Erickson, Z. Jia, S. P. Gross, C. C. Yu, How molecular motors are arranged on a cargo is important for vesicular transport. *PLoS Comput Biol* **7**, e1002032 (2011).
25. G. Arpag, S. Shastry, W. O. Hancock, E. Tuzel, Transport by populations of fast and slow kinesins uncovers novel family-dependent motor characteristics important for in vivo function. *Biophys J* **107**, 1896-1904 (2014).
26. S. S. Rosenfeld, P. M. Fordyce, G. M. Jefferson, P. H. King, S. M. Block, Stepping and stretching. How kinesin uses internal strain to walk processively. *J Biol Chem* **278**, 18550-18556 (2003).
27. Q. Li, S. J. King, A. Gopinathan, J. Xu, Quantitative Determination of the Probability of Multiple-Motor Transport in Bead-Based Assays. *Biophys J* **110**, 2720-2728 (2016).
28. R. J. McKenney, W. Huynh, M. E. Tanenbaum, G. Bhabha, R. D. Vale, Activation of cytoplasmic dynein motility by dynactin-cargo adapter complexes. *Science* **345**, 337-341 (2014).
29. G. Y. Chen, D. F. Arginteanu, W. O. Hancock, Processivity of the kinesin-2 KIF3A results from rear head gating and not front head gating. *J Biol Chem* **290**, 10274-10294 (2015).
30. A. M. Sendecki, M. F. Poyton, A. J. Baxter, T. Yang, P. S. Cremer, Supported Lipid Bilayers with Phosphatidylethanolamine as the Major Component. *Langmuir* **33**, 13423-13429 (2017).
31. A. M. Gicking *et al.*, The Orphan Kinesin PAKRP2 Achieves Processive Motility via a Noncanonical Stepping Mechanism. *Biophys J*, (2019).
32. J. Schindelin *et al.*, Fiji: an open-source platform for biological-image analysis. *Nature methods* **9**, 676 (2012).